Composites Part C: Open Access 20 (2026) 100718

Contents lists available at ScienceDirect

Composites Part C: Open Access

journal homepage: www.sciencedirect.com/journal/composites-part-c-open-access

Sustainable resin development for the strategic upcycling of waste fly ash into high-performance polymer composites

Giseok Park [a], Sunanda Roy [a], Jung Woong Kim [a], Hyun Chan Kim [b,*], Jaehwan Kim [a,*]

[a] CRC for Nanocellulose Future Composites, Mechanical Engineering, Inha University, 100 Inha-Ro, Incheon 22212, South Korea
[b] Department of Mechanical System Engineering, Kumoh National Institute of Technology (KIT), Kumi, Gyeongbuk 39177, South Korea

ARTICLE INFO

Keywords:
Eco-friendly resin
Polymer composites
Fly ash
Upcycling

ABSTRACT

Recently, there has been an increasing demand for Eco-friendly resins as alternatives to petroleum-based products to achieve carbon neutrality and reduce greenhouse gas emissions. Simultaneously, effective waste management is essential for promoting environmental sustainability. This study aims to address both issues by presenting the development of a novel high-performance Eco-friendly resin and its application in fly ash (FA)-based composites. The Eco-friendly resin was synthesized with sodium lignosulfonate, polyvinyl alcohol, and citric acid (CA), a crosslinker. The optimal resin properties were determined by varying the CA concentration and crosslinking conditions, and esterification was performed. This reaction resulted in significant improvements of the esterified resin in tensile strength (127.8 %), Young's modulus (36.6 %), toughness (1237.8 %), elongation (420.4 %), and hydrophobicity (44.3 %), compared to the hydrogen-bonded resin. The FA was modified using polydopamine, a biomimetic self-adhesive polymer, to enhance interfacial compatibility and facilitate the formation of covalent ester crosslinks with the matrix, alongside physical interactions. Subsequently, chemically modified FA (M-FA) with different concentrations was blended with this resin to produce composites. Notably, the incorporation of only 0.1 wt.% of M-FA into the lignin-based resin resulted in a significant increase in tensile strength (38.5 %), elongation at break (12.5 %), Young's modulus (27.6 %), and toughness (65.4 %) compared to the unmodified FA(U-FA) composites. While conventional approaches have historically shown poor FA–polymer composites, our novel approach presents a transformative opportunity to convert fly ash into high-performance composite materials, defined by a tensile strength exceeding 140 MPa and thermal stability comparable to engineering plastics.

1. Introduction

Increasing environmental concerns worldwide are driving research into developing environmentally friendly materials. The depletion of conventional fossil fuels also drives the world towards developing lightweight, eco-friendly structural materials to replace petroleum-based products, as petroleum-based plastics generate significant carbon dioxide emissions during production and pyrolysis. In this context, Eco-friendly resins have gained considerable attention due to their renewable properties, reduced carbon emissions, and potential applications in circular economy models. Concurrently, the continuous accumulation of various wastes necessitates finding solutions to recycle and upcycle them to reduce our CO_2 footprint and mitigate global warming. Consequently, various efforts are underway in academia and industry to address these challenges. Structural materials reinforced by modifying Eco-friendly resins and potential wastes will, therefore, be of great interest.

Fly ash (FA), Coal combustion residuals (CCRs) have detrimental environmental effects due to their high generation rates and inadequate disposal methods. When FA is not properly managed, it can become airborne, leading to particulate matter pollution and inducing respiratory disorders and other detrimental health effects in both humans and animals. Moreover, FA can pollute the soil, landfills, and water bodies, eventually contributing to climate change. Until now, FA has primarily been used for construction applications [1,2]. Although there have been some studies on FA-based polymer composites, including recent investigations into ash-filled polymer systems [3,4], extensive research remains limited. Previous literature has shown that pristine FA significantly degrades the mechanical properties of composites, reducing their physical strength and durability [5–9]. Research by Pattanaik and

* Corresponding authors.
E-mail addresses: hyunckim@kumoh.ac.kr (H.C. Kim), jaehwan@inha.ac.kr (J. Kim).

https://doi.org/10.1016/j.jcomc.2026.100718

Available online 20 March 2026

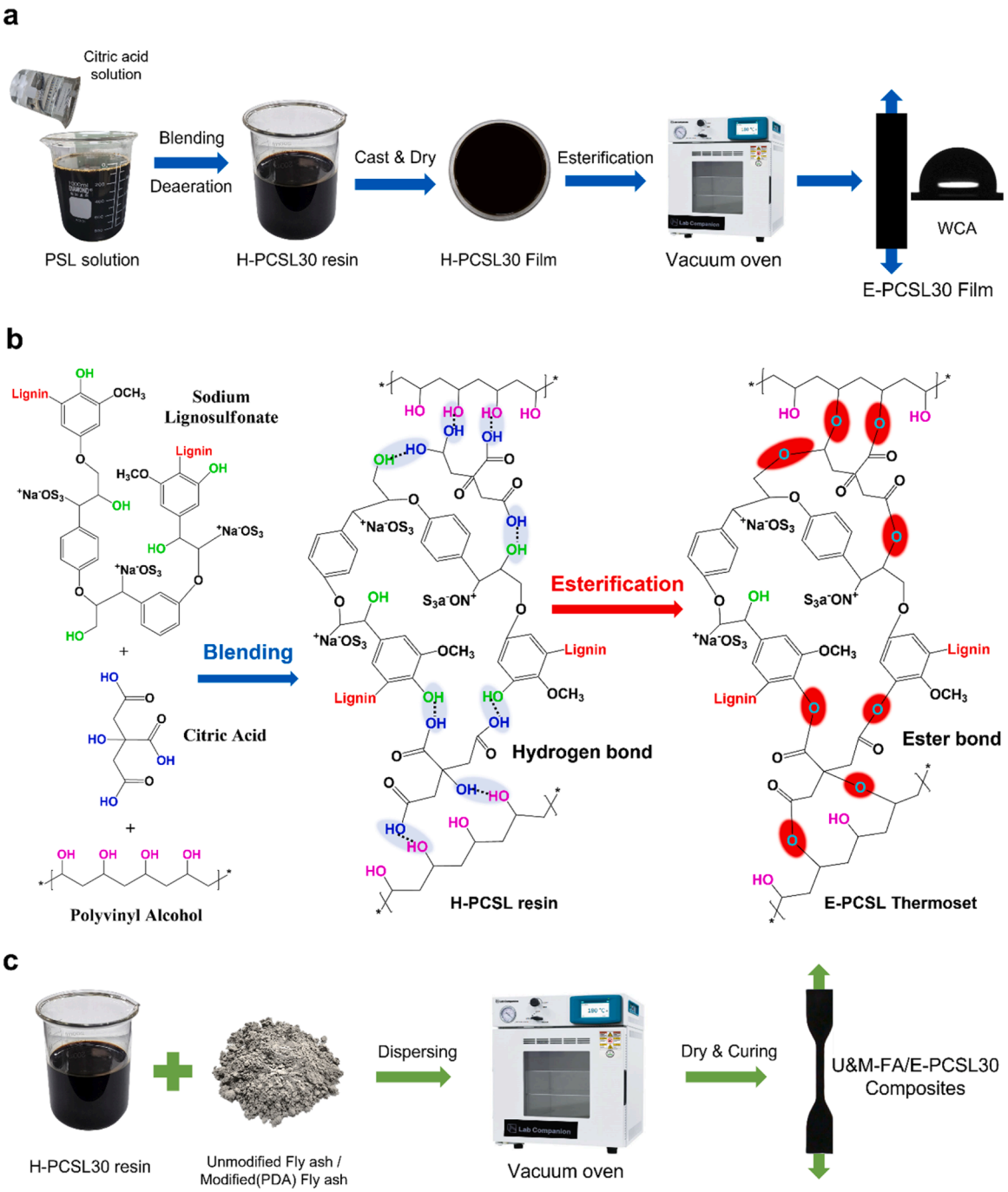

Fig. 1. (a) Illustration of synthesis and characterization of H-PCSL and E-PCSL resins. (b) Lignin-based resin processing of H-PCSL, E-PCSL resin synthesis, and esterification. (c) Fabrication procedure of U&M-FA/E-PCSL30 composites.

colleagues on LY556/HY951 epoxy systems demonstrated that incorporating a 10 % mass fraction of FA yielded optimal mechanical performance, specifically recording an ultimate tensile stress of 90.07 MPa coupled with a 2.87 % elongation [5]. Nevertheless, escalating the filler concentration to 40 % induced a substantial decline, dropping the strength and deformation limits to 61.77 MPa and 1.97 %, respectively. In a comparative analysis, Altaweel et al. investigated both neat and silicone-toughened LY556 matrices containing FA [6]. Testing of the control (unmodified) epoxy revealed an elastic modulus of 1.5 GPa alongside a maximum tensile stress of 61 MPa. Blending 15 phr of FA into this pristine matrix severely compromised its structural integrity, lowering the modulus to 0.8 GPa and the strength to 38 MPa. For the silicone-modified variant, the initial parameters were measured at 1.3 GPa for stiffness and 43 MPa for tensile capacity. However, with 15 phr FA, these values further decreased to 21 MPa and 0.6 GPa, respectively. Gnanavel et al. studied composites of epoxy resin (LY556) with both coarse and fine FA [7]. While the reference epoxy withstood up to 75 MPa with an elongation of 2.1 %, the dispersion of 5 wt % coarse FA reduced these metrics to 65 MPa and 1.9 %. In contrast, substituting coarse particles with fine FA at identical weight percentages mitigated this mechanical degradation slightly, preserving a strength capacity of 68 MPa and a 2.0 % strain. Wongwuttanasatian et al. investigated composites using epoxy resin (200A), hardener (200B), and FA modified by silane coupling [8]. The blank resin displayed a stiffness of 0.50 GPa and failed at 55.95 MPa under tension. The integration of 25 % untreated FA (U-FA) triggered a massive reduction in tensile capacity

(down to 18.09 MPa) and slightly lowered the modulus (0.49 GPa). Although applying a silane coupling agent to the FA surface facilitated a partial recovery—yielding 0.77 GPa in modulus and 24.73 MPa in strength—the overall properties failed to surpass those of the neat polymer. This indicates the challenges associated with FA in preparing effective composites.

FA has a porous, hydrophilic structure, which results in high moisture absorption. Additionally, FA particles vary in size and possess complex surface chemistry, which often results in poor interfacial compatibility with many polymers [10]. Thus, creating desirable composites with FA presents considerable challenges. These limitations hinder the utilization of FA in polymer composites. To address these limitations, surface modification of FA was carried out. Functionalization with polydopamine (PDA) was found to significantly enhance the interfacial bonding, facilitate densification, introduce cross-linking capability, and improve compatibility with the Eco-friendly resin. The intricate surface chemistry of FA, caused by the presence of metal species and residual carbon, makes direct chemical modification challenging. To overcome this, PDA was employed as an effective surface modifier, as it forms a uniform coating on FA particles and enhances interfacial adhesion with the matrix through its abundant polar functional groups [11]. PDA has been widely recognized as an effective interfacial adhesion promoter for nanomaterials in composite systems [12,13]. In our study, FA modified with a PDA coating provided significantly stronger reinforcement than unmodified FA.

Given these challenges, this paper presents a novel process for synthesizing a strong Eco-friendly resin and FA composite. An innovative Eco-friendly resin was developed and then combined with PDA-modified FA (M-FA). The resin, named E-PCSL (Esterified-PVA/CA/SL), is composed of esterified polyvinyl alcohol (PVA), citric acid (CA), and sodium lignosulfonate (SL). The resin was specifically designed to impart high strength to the composites. Firstly, the resin properties were optimized by varying the CA content, a well-known natural crosslinking agent [14]. Subsequently, FA was incorporated into the resin at various loading levels to develop high-performance M-FA/E-PCSL composites. Consequently, the resulting materials exhibited a substantial improvement in their thermal and mechanical performance. Notably, both PVA and SL are biodegradable biopolymers, with SL being a renewable polymer derived from lignin and offering a more cost-effective alternative to kraft lignin [15]. A comprehensive investigation was conducted covering resin synthesis, FA functionalization, and composite fabrication. Although consuming a higher proportion of waste-based FA is highly desired from an environmental perspective, our preliminary evaluations indicated that excessive filler loading inevitably induces severe particle agglomeration, critically deteriorating the mechanical integrity. Therefore, this study systematically investigated the effect of FA concentration (up to 2.5 wt.%) to identify the exact optimal loading (0.1 wt.%) that maximizes the reinforcing efficiency of M-FA while strictly preserving the structural robustness of the composite. The results demonstrate that with appropriate material design and strategic integration, hazardous FA can be effectively transformed into a valuable resource for future sustainable structural applications.

2. Materials and methods

2.1. Materials

The citric acid (99 %) was sourced from Sigma-Aldrich Co. (USA), Sodium lignosulfonate (Alkaline lignin pH 8.0 to 10.0) was purchased from TCI (Japan), with a Poly ((vinyl alcohol) 99 % hydrolyzed) weight spanning the 84,000–124,000 g/mol range was procured from Sigma-Aldrich (USA). The raw fly ash, possessing an average grain size of 100.6 μm, was obtained from Kosep Materials Company (South Korea).

2.2. Preparation of PVA, SL, and CA solution

The resin synthesis was carried out in multiple steps. First, 100 g of PVA was dissolved in 900 g of deionized water to prepare a 10 wt.% solution. Separately, 30 g of sodium lignosulfonate (SL) powder was dispersed in 270 g of deionized water and homogenized using an ultrasonicator (HD 2200, Bandelin Electronic Co., Germany) at 70 % power for 1 min, followed by magnetic stirring for 1 h, yielding a 10 wt.% SL solution. The PVA and SL solutions were then mixed in a 70:30 ratio and stirred magnetically for 6 h, followed by an additional 30 min using an ultra-sonicator at 60 % power in a chilled ice-water bath. Finally, the mixture was stirred continuously for another 12 h to ensure thorough blending.

2.3. Preparation of H-PCSL and E-PCSL resins

Fig. 1a illustrates the preparation of H-PCSL and E-PCSL resins. The hydrogen-bonded PVA/CA/SL (H-PCSL) resin was blended at 10 wt% CA in a PSL solution in the following ratios: 5, 10, 15, 20, 30, and 40 wt %. After thorough mixing with CA on a magnetic stirrer for 1 h, the H-PCSL resin was further homogenized in an ice bath using an ultrasonicator for 20 min (the ice bath was employed to minimize thermal effects). The homogenized resin was then cast into Petri dishes and dried at 24 °C (room temperature) for 36 h, followed by oven drying at 60 °C for another 30 h.

To accomplish the esterification, the H-PCSL films were heated in a vacuum oven at 180 °C for 18 h to obtain E-PCSL (5 to 40 wt%) films ('E' stands for esterification). Fig. 1b shows the synthesis of H-PCSL and E-PCSL resin. Firstly, PVA and SL were mixed with CA to form H-PCSL resin, which was later esterified at 180 °C to form E-PCSL resin. The hydrogen bonding interactions were dominant in the case of H-PCSL. After esterification, the covalent ester bond was formed in the E-PCSL resin, as shown in the schematic.

2.4. Preparation of modified FA (M-FA)

A Trizma buffer medium (200 mL, 50 mM, pH 8.7) was employed to suspend 20 g of raw FA at the start of the functionalization process. This initial dispersion was achieved through 10 min of acoustic cavitation utilizing a probe-type ultrasonicator (Bandelin Electronics, Berlin; 20 kHz, 200 W, 65 % efficiency). Subsequently, 2 g of dopamine hydrochloride was incorporated into the suspension. The functionalization reaction was allowed to proceed under continuous magnetic agitation for 10 h at a regulated temperature of 45 °C. The successful in-situ polymerization of dopamine into a polydopamine (PDA) layer was visually evidenced by a stark color transition in the mixture, shifting from its original grey to a dark brown hue. Importantly, the application of ultrasonic energy during this modification stage successfully hindered particle clustering, ensuring that the inherent nano-to-micro size distribution of the FA fillers remained intact. Ultimately, the PDA-decorated particles (M-FA) were isolated via vacuum filtration using an 8.0 μm pore-size filter membrane (190 μm thickness) and underwent exhaustive rinsing with deionized water to extract any unreacted dopamine residues. An in-depth morphological and chemical characterization of this synthesized M-FA can be found in our earlier publication [16].

2.5. Fabrication of M-FA/E-PCSL composites

Diverse M-FA loadings (0.1, 0.25, 0.5, 1.25, and 2.5 wt.%) were incorporated into the H-PCSL system, as illustrated in the schematic (Fig. 1c). To initiate the mixing process, the M-FA/resin blend was subjected to magnetic stirring for a 1 h duration, which was then complemented by a subsequent ultrasonic homogenization step for further refinement. The homogenized M-FA/H-PCSL was poured into a petri dish and allowed to solidify under ambient conditions for a 24 h period.

Table 1
Formulations of U-FA and M-FA reinforced E-PCSL composites.

Composite name	PVA(g)	CA(g)	SL(g)	FA(g)	Total dry weight(g)
U-FA 0.1	14.55	8.91	6.24	0.3	30
M-FA 0.1	14.55	8.91	6.24	0.3	30
M-FA 0.25	14.33	8.78	6.14	0.75	30
M-FA 0.5	13.97	8.55	5.99	1.5	30
M-FA 1.25	12.86	7.88	5.51	3.75	30
U-FA 2.5	11.03	6.75	4.73	7.5	30
M-FA 2.5	11.03	6.75	4.73	7.5	30

Next, the samples were placed between two metal plates (to avoid structural deformation) and heated at 180 °C for 18 h under vacuum to drive the esterification reaction to completion. It should be noted that during the composite synthesis, the E-PCSL30 resin was selected, as the resin with 30 % citric acid content proved to be the most effective. M-FA/E-PCL30 composite is named as M-FAx, where x represents the weight percent of M-FA. The composite formulations are summarized in Table 1.

2.6. Characterizations

Chemical configurations of both the pristine E-PCSL matrix and the M-FA specimens were elucidated via Fourier transform infrared spectroscopy (FTIR, Bruker Optics, USA). Following a rigorous oven-drying step to eliminate moisture, spectral data were collected across a 550–4000 cm^{-1} sweep. These measurements incorporated both transmission and attenuated total reflectance (ATR) modes, compiling 16 consecutive scans at a spectral resolution of 4 cm^{-1}. Thermal degradation behaviors were monitored using a TG 209 F3 Tarsus thermogravimetric apparatus (Germany). The samples were subjected to a constant heating ramp of 10 °C/min, spanning a temperature window of 35 to 600 °C within a continuous nitrogen flow. For morphological investigations, the surface topographies of the fabricated films were inspected through field-emission scanning electron microscopy (FE-SEM, SU8010, Hitachi, Japan). Additionally, dynamic thermo-mechanical responses were captured using a TA Instruments Q800 dynamic mechanical analyzer (USA). The testing was executed in a tensile configuration, sweeping temperatures from 40 to 160 °C at a 5 °C/min heating trajectory, while maintaining a constant oscillatory frequency of 1 Hz and a 10 μm strain amplitude. The average thickness of PSL, H-PCSL, and E-PCSL resin films was 0.1384 ± 0.002 mm, while that of U-FA and M-FA composite films was 0.1526 ± 0.003 mm. Mechanical properties were evaluated using a tensile testing machine (T0–102C) under conditions of 24 °C and 40 % relative humidity, in accordance with the ASTM D638 standard. For each composition, a minimum of five samples were evaluated at a displacement rate of 2.5 mm/min to verify data reliability. The reported numerical values (strength, modulus, elongation, and toughness) represent the mean ± standard deviation, while the stress-strain curves presented in Figs. 4 and 5 are representative curves selected to best reflect the average behavior of each sample group. Eight samples were

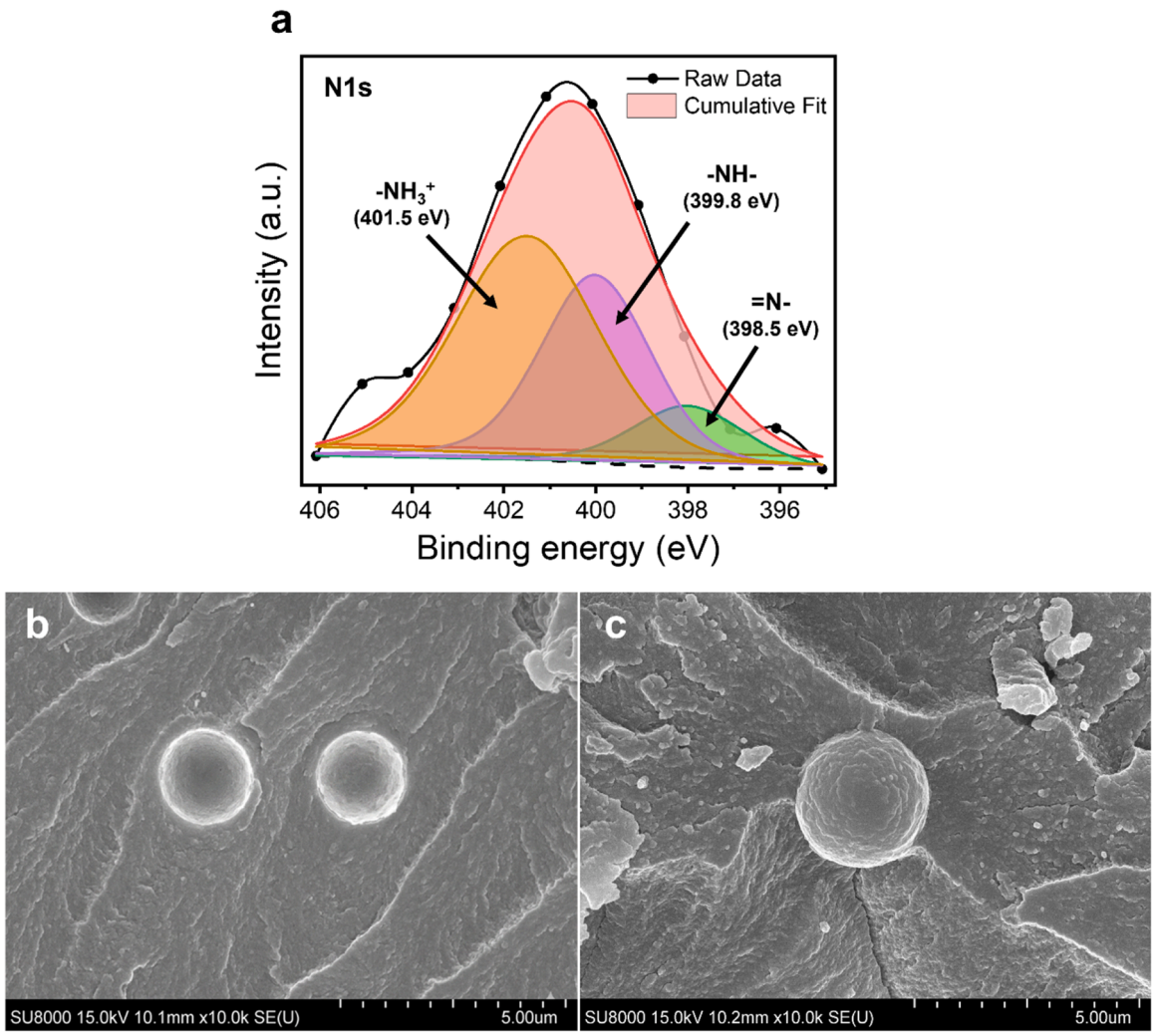

Fig. 2. Surface characterization: (a) N1s XPS spectrum of M-FA, SEM images showing the surface morphology of (b) U-FA and (c) M-FA.

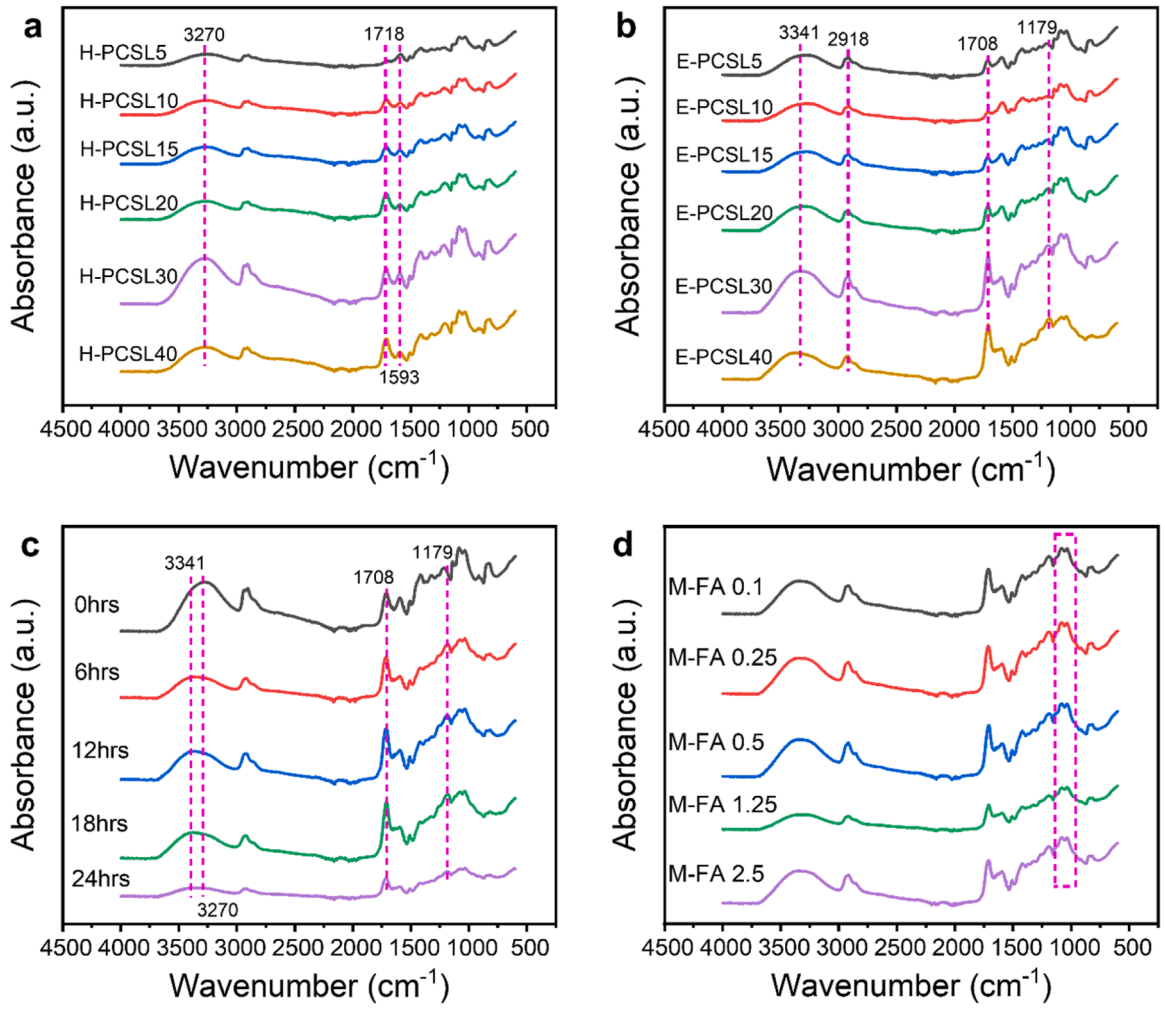

Fig. 3. FTIR of (a) H-PCSL, (b) E-PCSL resin, (c) E-PCSL30 resin by esterification time, (d) M-FA/E-PCSL30 composite.

tested from each composite, and the average values were presented. To evaluate the surface wettability of both the pristine matrices and the M-FA composites, water contact angle (WCA) measurements were conducted utilizing a GSA optical tensiometer (Surfacetech Co., Korea). Individual test specimens were securely mounted onto glass substrates prior to analysis. For each evaluation, a precise water droplet with a volume of approximately ~ 8 μL. was dispensed onto the target surface. To guarantee data consistency and statistical reliability, the final WCA values reported herein reflect the arithmetic mean of six independent trials for each sample formulation.

3. Results and discussion

3.1. Characterization of M-FA

To verify the successful introduction of the PDA layer on the FA surface, XPS analysis was performed first. Fig. 2a presents the high-resolution N1s spectrum of M-FA. Since U-FA exhibited a negligible N1s signal consistent with previous reports [16], only the deconvoluted M-FA spectrum is displayed to highlight the specific nitrogen functional groups. Through peak deconvolution of the N1s spectrum, this signal can be assigned to the amine (-NH-) and imine (=N-) groups, which are characteristic functional groups of polydopamine. This dramatic emergence of nitrogen confirms that the PDA was chemically coated onto the FA surface.

This chemical modification is visually supported by the morphological changes observed in the SEM images presented in Fig. 2b-c. The U-FA (Fig. 2b) shows a smooth and spherical surface typical of pristine cenospheres. However, after the PDA coating process in the buffer solution, the surface morphology changes significantly. As shown in Fig. 2c, the M-FA exhibits a rougher texture with a continuous organic layer and granular aggregates. These SEM observations, combined with the XPS results, conclusively demonstrate that the PDA layer was successfully synthesized and deposited on the FA surface via oxidative self-polymerization.

3.2. FTIR

The FTIR spectra of the prepared H-PCSL and E-PCSL resins were evaluated to understand the effects of CA on the resin formation. Fig. 3a-b show the FTIR spectra of all H-PCSL (before esterification) and E-PCSL resins (after esterification) containing CA from 5 to 40 wt%. A comparative evaluation of the spectral data highlighted distinct chemical alterations. Focusing on the neat sodium lignosulfonate, the structural profile displayed fundamental signature bands: the primary hydroxyl (-OH) stretching mode was centered at 3270 cm^{-1}, whereas the symmetric aliphatic -CH stretching vibrations appeared at 2905 cm^{-1}. Furthermore, the characteristic symmetric S=O stretch associated with the sulfonate ($-SO_3$) functionalities was clearly resolved at 1034 cm^{-1} [17]. As hydrogen bonds are formed, the O—H stretching peaks appearing at 3200–3600 cm^{-1} become larger or broader in range, and the intensity of the O—H peak increases with the loading of the CA crosslinker. The esterification of H-PCSL triggered a substantial migration of the O—H stretching signals (3200–3600 cm^{-1}) toward a higher

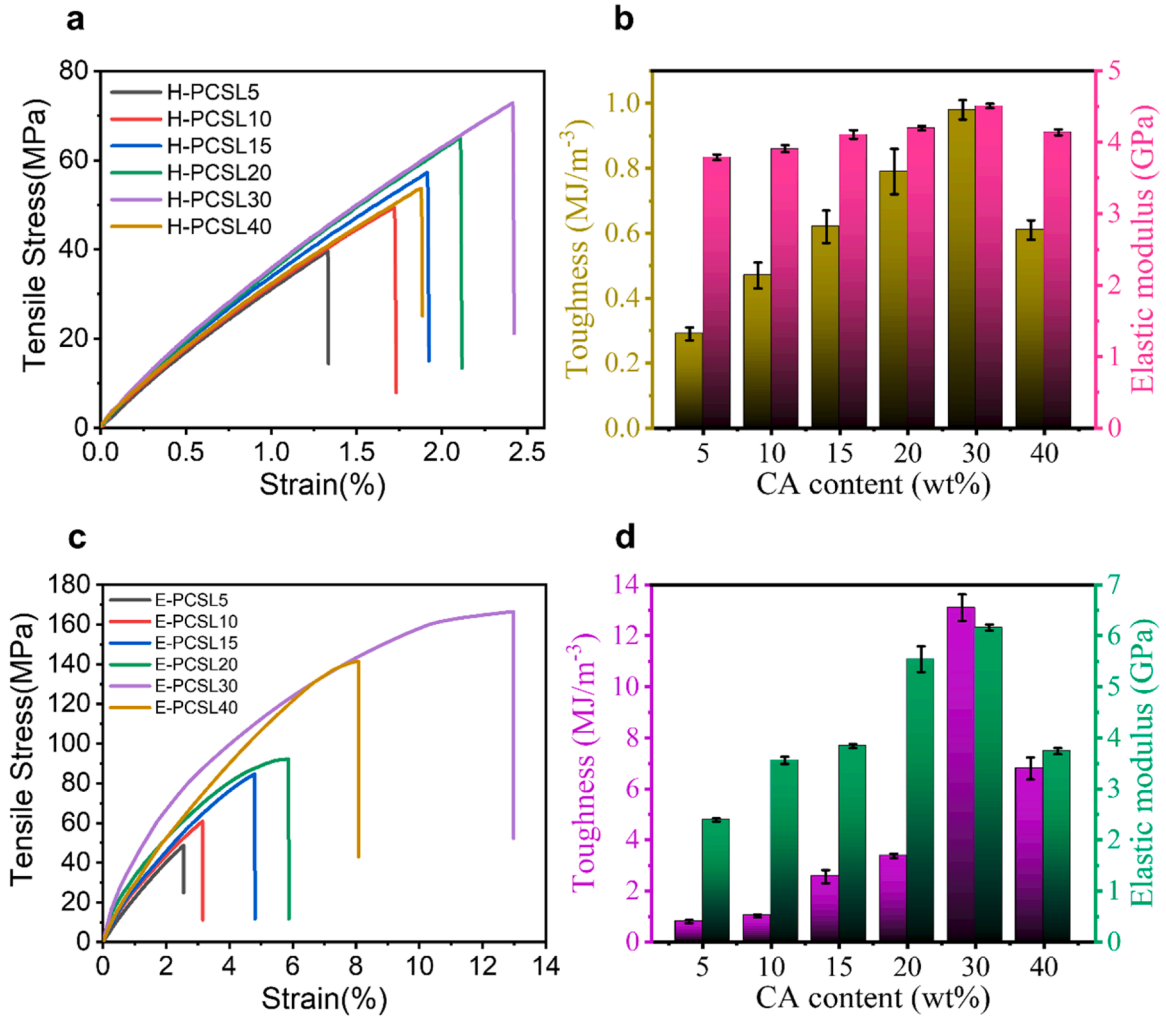

Fig. 4. Mechanical properties of H-PCSL and E-PCSL resins: (a, c) Characteristic tensile stress-strain profiles, and (b, d) toughness and Young's modulus values.

wavenumber of 3341 cm^{-1} (Fig. 3b). This spectral change, coupled with a reduction in peak magnitude, is primarily attributable to the conversion of intermolecular hydrogen bonds into covalent C—O stretching vibrations inherent in the ester structure. The emergence of a sharp keto peak (-C=O) at 1708 cm^{-1} also indicates the formation of covalent esterification (Fig. 3b) [18]. This peak intensity was found to be the maximum for E-PCSL30 resin. Moreover, the intensity of the C—O stretching peak between 1000 and 1250 cm^{-1} increased. These changes indicate the successful formation of esterification between H-PCSL resin and CA.

Next, the effects of esterification time, ranging from 0 to 24 h on the E-PCSL30 resin, were examined (Fig. 3c). As the esterification process progressed over time, a more robust coupling between the -COOH and -OH moieties were established. Consequently, the infrared spectra displayed a significant growth in peak magnitude for both the ester carbonyl (-COO) and the -CH stretching mode centered at 2918cm^{-1}. However, overheating can impair the esterification process, leading to a decrease in the C—O stretching peak, as observed in the 24 h treatment. Based on the FTIR results, 18 h was determined as the optimal esterification time for all crosslinker contents. Then, composites were prepared using different contents of M-FA with E-PCSL30 resin cured at 18 h, and the corresponding FTIR spectra are presented in Fig. 3d. Regarding the high-content M-FA2.5 formulation, the characteristic band in the 950–1100 cm^{-1} range migrated toward a lower wavenumber and exhibited a broader distribution. This specific absorption arises from the asymmetric vibrational signatures of the Si–O–T (T = Si or Al) structural units. Although the absolute absorbance is slightly lower than that of samples containing a small amount of M-FA, the changes in peak shape and position indicate that aluminum has been introduced into the silicate framework to form Al–O–Si bonds and create a more diverse network structure. These changes signify the development of an aluminosilicate network with increased aluminum substitution.

3.3. *Mechanical properties of resins*

The mechanical properties of the resin were investigated. Fig. 4a presents the stress-strain behavior of E-PCSL with varying CA contents (0–40 wt%). As evidenced by the data in Table 2 and Fig. 4a–d, the esterification process at 180 °C effectively enhances the mechanical properties, showing marked increases in maximum tensile capacity, ductility, material rigidity, tensile modulus, and fracture toughness. As CA content increased up to 30 wt%, the toughness of the resin exhibited a significant improvement. Fundamentally, this mechanical upgrade is driven by the creation of a dense non-covalent architecture, wherein extensive hydrogen bonds link the prolific carboxyl and hydroxyl functionalities of the CA with the constituent PVA/SL polymer chains. Under external stress, these non-covalent interactions effectively dissipate energy by breaking and reforming prior to the rupture of the covalent backbone. Furthermore, excess CA likely acts as a plasticizer, increasing the free volume between polymer chains, which facilitates chain slippage and elongation. Consequently, this concerted mechanism of energy dissipation and enhanced chain flexibility results in the

Table 2
Benchmarking the mechanical performance of PCSL resins against previously reported values in the literature.

Lignin network	$\sigma_{tensile}$ (MPa)	$\varepsilon_{tensile}$ (%)	$E_{tensile}$ (GPa)	$U_{tensile}$ (MJ/m^{-3})	Ref.
H-PCSL40	57.76 ± 2.73	2.04 ± 0.04	4.14 ± 0.04	0.61 ± 0.03	Current
E-PCSL40	149.80 ± 0.21	8.20 ± 0.43	3.74 ± 0.06	6.80 ± 0.43	Current
H-PCSL30	**72.47 ± 0.83**	**2.50 ± 0.08**	**4.51 ± 0.03**	**0.98 ± 0.03**	**Current**
E-PCSL30	**165.09 ± 2.65**	**13.01 ± 0.02**	**6.16 ± 0.06**	**13.10 ± 0.52**	**Current**
H-PCSL20	65.01 ± 1.62	2.29 ± 0.12	4.20 ± 0.03	0.79 ± 0.07	Current
E-PCSL20	90.34 ± 2.86	6.43 ± 0.17	5.54 ± 0.25	3.37 ± 0.09	Current
H-PCSL15	57.85 ± 1.03	2.15 ± 0.04	4.11 ± 0.06	0.62 ± 0.05	Current
E-PCSL15	82.49 ± 1.93	5.23 ± 0.59	3.84 ± 0.04	2.56 ± 0.26	Current
H-PCSL10	48.91 ± 2.36	2.08 ± 0.05	3.91 ± 0.05	0.46 ± 0.03	Current
E-PCSL10	67.85 ± 3.36	2.95 ± 0.01	3.56 ± 0.07	1.02 ± 0.06	Current
H-PCSL5	39.95 ± 0.64	1.84 ± 0.05	3.79 ± 0.04	0.29 ± 0.02	Current
E-PCSL5	57.43 ± 3.74	2.83 ± 0.18	2.39 ± 0.03	0.81 ± 0.07	Current
PVA-SL30	106.39 ± 1.08	6.60 ± 0.36	3.72 ± 0.10	4.09 ± 0.23	Current
S-PCL [a)]	12.06 ± 0.69	3.22 ± 0.16	0.59 ± 0.07	-	[19]
L/C [b)]	18.71	1.8~2	1.7~2	-	[20]
PVA-Lignin	41.1 ± 1.6	2.49 ± 0.23	2.48 ± 0.1	-	[21]
E-P-L-MA40 [c)]	48.5 ± 6.2	2.7 ± 0.3	2.4 ± 0.2	0.78 ± 0.11	[18]
Lignin-Epoxy	67.5 ± 7.93	4.7 ± 1.13	3.38 ± 0.16		[22]
E-SCL40 [d)]	158.79 ± 6.51	7.28 ± 0.18	3.31 ± 0.18	6.26 ± 0.39	[23]

[a] S-PCL - Lignosulfonate Polycaprolactone.
[b] L/C – Sodium lignosulfonate/Chitosan.
[c] Esterification PVA/Kraft lignin/Malic acid.
[d] E-SCL – Esterification Starch/Citric acid/Kraft lignin.

superior toughness observed. Compared to H-PCSL30, the formulation experienced remarkable relative surges in its elastic modulus, maximum tensile stress, stretchability, and fracture toughness by 36.6 %, 127.8 %, 420.4 % and 1237.8 %, respectively. As presented in Table 2, previous studies on lignin-based resins, such as Lignosulfonate/Polycaprolactone [19], Sodium Lignosulfonate/Chitosan [20], PVA-Lignin [21], esterified PVA-Lignin-Malic acid [18], Lignin-Epoxy [22], and esterified Starch/-Citric acid/Lignin [23], have reported tensile strengths of 12.06, 18.71, 41.1, 48.5, 67.5, and 158.79 MPa, respectively. In contrast, the E-PCSL30 resin developed in this study demonstrates significantly higher mechanical strength, underscoring its outstanding potential as a high-performance Eco-friendly resin for composite applications.

3.4. Mechanical properties of M-FA/E-PCSL30 composites

Fig. 5a shows stress-strain curves of the M-FA/E-PCSL30 composites. While unmodified fly ash(U-FA) led to brittle and weak composites, the inclusion of M-FA markedly improved mechanical performance. The composite with 0.1 wt.% M-FA in the E-PCSL30 matrix (M-FA0.1) exhibited the largest tensile strength, Young's modulus, and toughness. However, further increasing the FA content led to a decline in performance due to particle agglomeration and bottom precipitation of the resin. Nonetheless, in comparison to the U-FA composite at 2.5 wt.% (U-FA2.5), the M-FA2.5 demonstrated remarkable improvements: tensile strength increased by 283.73 %, elongation at break by 327.42 %, Young's modulus by 53.60 %, and toughness by 1984.62 % (Fig. 5b). Although the mechanical properties of the M-FA0.1 composite were slightly lower than the E-PCSL30 pure resin, the composite still maintained considerable structural strength. Moreover, our composites outperformed many recently reported systems [5–9,24–27]. These findings highlight the importance of FA surface modification, which enables effective reinforcement and partial recovery of the resin's intrinsic strength, an outcome unattainable with unmodified FA-based composites. The significant reinforcement achieved at such a low loading (0.1 wt.%) is attributed to the optimal critical dispersion limit where M-FA particles are individually dispersed, acting as effective stress transfer centers without agglomeration. Crucially, the PDA coating is instrumental in this enhancement. A high density of catechol and amine moieties within the PDA coating promotes resilient interfacial engagement—primarily mediated by hydrogen bond coupling and π-stacking—with the resin matrix. This molecular bridging effect guarantees enhanced bonding integrity at the filler-matrix junction, which is critical for seamless load distribution. In stark contrast, as summarized in Table 3, conventional approaches reported in the literature typically required much higher filler loadings, such as 5–10 wt.% or 5 phr. but failed to achieve comparable mechanical strength [5–9,24–27]. These previous composites often suffered from poor interfacial compatibility and particle agglomeration, which served as defect points rather than reinforcement. Our results, achieving a tensile strength of 144.8 MPa

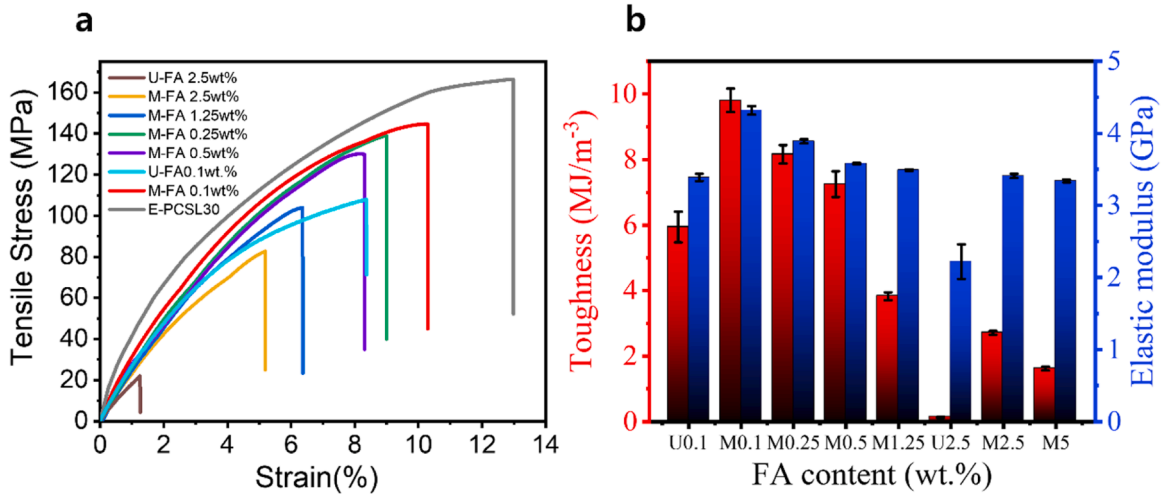

Fig. 5. Mechanical properties of U, M-FA/E-PCSL30 composites: (a) Representative stress-strain curves, and (b) toughness and Young's modulus values.

Table 3
Mechanical properties of pure resin and FA/E-PCSL30 composites as a function of FA content, compared with selected literature data.

Composite name	$\sigma_{tensile}$ (MPa)	$\varepsilon_{tensile}$ (%)	$E_{tensile}$ (GPa)	$U_{tensile}$ (MJ/ m^{-3})	Ref.
M-FA0.1	**144.79 ± 0.42**	**9.53 ± 0.95**	**4.32 ± 0.06**	**9.81 ± 0.86**	**Current**
U-FA0.1	**104.57 ± 4.54**	**8.47 ± 0.34**	**3.39 ± 0.05**	**5.93 ± 0.47**	**Current**
M-FA0.25	140.52 ± 1.06	9.36 ± 0.28	3.91 ± 0.03	8.16 ± 0.28	Current
M-FA0.5	134.70 ± 1.49	9.04 ± 0.54	3.58 ± 0.01	7.25 ± 0.49	Current
M-FA1.25	101.11 ± 1.98	6.46 ± 0.35	3.49 ± 0.01	3.83 ± 0.12	Current
M-FA2.5	**84.83 ± 1.49**	**5.30 ± 0.08**	**3.41 ± 0.03**	**2.71 ± 0.06**	**Current**
U-FA2.5	**22.13 ± 0.4**	**1.24 ± 0.19**	**2.22 ± 0.24**	**0.13 ± 0.02**	**Current**
FA15 %/HDPE	29.3	-	1.93	-	Thermoplastic [24]
PVC/FA8phr	64.57	7 ≈	0.7≈	-	Thermoplastic [25]
FA-10phr[a)]	31.62 ± 0.41	-	-	-	Thermoplastic [26]
CMC-FA[b)]	34.63	-	1.08	12.12	Thermoplastic [27]
Epoxy-FA10wt %[c)]	90.07	2.87	-	-	Thermoset [5]
Epoxy+5phr FA[d)]	45	-	1.0	-	Thermoset [6]
Epoxy+C-FA1wt%[e)]	72	2.2	-	-	Thermoset [7]
Treated-5wt% FA[f)]	46.51		0.615		Thermoset [8]
Epoxy+FA10wt %[g)]	113.57	3.62	-	-	Thermoset [9]

[a] FA-10phr - Polyolefin elastomer 20phr/ Polypropylene grafted with maleic anhydride 5phr/FA 10phr.
[b] CMC-FA - Carboxymethyl cellulose/FA.
[c] Epoxy-FA10wt.% - LY 556/HY951/FA 10 wt.%,.
[d] Epoxy+5phr FA - LY 556/HY951/HT972/FA 5phr.
[e] Epoxy+C-FA1wt.% - LY 556/HY951/C class-FA 1wt%.
[f] Treated-5wt%FA - Diglycidyl ether of Bisphenol-A/ Isophorone Diamine/ Silane treated FA 5 wt.%.
[g] Epoxy+FA10wt% - LY 556/HY951/F class-FA 10wt%.

with minimal filler, validate the transformative nature of this study: by overcoming the historical limitations of poor FA polymer interfaces through polydopamine-mediated functionalization, we have successfully converted industrial waste into a truly high-performance composite material.

3.5. Morphologies

Fig. 6 compares the fracture morphologies of the pure resin and the FA composites. The fracture surface of the pure E-PCSL30 resin (Fig. 6a) exhibits a typically smooth and flat morphology, indicating brittle failure behavior.

For the U-FA composites (Fig. 6b-c), distinct phase separation and poor dispersion are observed. As clearly shown in Fig. 6b, the U-FA fillers tend to settle to the bottom (sedimentation) due to the density difference and lack of compatibility with the E-PCSL30 resin matrix [28]. Furthermore, the high-magnification view in Fig. 6c reveals that the particles are agglomerated rather than dispersed. The voids left by particle pull-out exhibit smooth and clean surfaces with clear gaps between the filler and the matrix. This morphology indicates weak interfacial adhesion, where the failure primarily occurred at the interface (adhesive failure).

In significant contrast, the M-FA composites (Fig. 6d–h) demonstrate improved dispersion and enhanced interfacial interaction. In the composite with the lowest M-FA content (Fig. 6d), the particles are homogeneously dispersed throughout the E-PCSL30 resin matrix without the sedimentation observed in the U-FA samples. Notably, the matrix surrounding the embedded particles displays extensive plastic deformation and prominent tearing ridges (sunburst-like pattern). Unlike the smooth voids in Fig. 6c, the rough texture in Fig. 6d suggests that the polymer chains were significantly stretched and yielded during fracture due to the strong anchoring effect of the PDA layer. This confirms that the applied stress was effectively transferred across the interface, leading to cohesive failure within the matrix rather than simple interfacial debonding. As the filler content increases (Fig. 6e–h), the particles remain relatively well-dispersed, maintaining the rough fracture surface characteristics indicative of good compatibility.

3.6. Thermal properties

The thermal stability, a crucial aspect of eco-friendly polymers intended to replace conventional petroleum-based polymers, was illustrated in Fig. 7. The TGA was performed on various E-PCSL resins (Fig. 7a) and M-FA/E-PCSL30 composites (Fig. 7b), revealing a multi-step thermal decomposition behaviour. The desorption of physically adsorbed water accounts for the initial weight reduction below 150 °C. A secondary mass loss event is observed in the temperature window of 220–350 °C, driven by the thermal deterioration of functional moieties such as C—O, -C=O, COOH, S=O, and aliphatic C—H linkages [29]. As the heating progresses past 350 °C, the macromolecular skeleton undergoes extensive chain scission and depolymerization, ultimately culminating in the accumulation of a solid char residue [30]. Regarding the effect of CA content, a trade-off was observed between early-stage stability and high-temperature resistance. The shift of $T_{d10\ \%}$ to lower temperatures is chemically driven by the intramolecular dehydration of citric acid to form anhydrides, along with the catalytic degradation of oligomers induced by acidic conditions. Conversely, the significant increase in $T_{d50\ \%}$ is a direct consequence of the ester-crosslinked network. This rigid structure restricts polymer chain mobility and promotes the formation of a thermally stable char layer, which acts as an insulating barrier against heat propagation.

The decomposition temperature at $T_{d10\ \%}$ increased with the incorporation of M-FA, attributed to the interaction between phenolic groups (aromatic rings, hydroxyl, and alkali groups) present in SL and the silica and alumina groups in M-FA. This bonding enhances thermal stability, resulting in higher degradation temperatures at both $T_{d10\ \%}$ and $T_{d50\ \%}$ [31,32].

Fig. 7a-b present the DTG curves, highlighting the major degradation stages. In Fig. 7a, the E-PCSL resin with an initial CA content of 5 wt.% undergoes two-stage degradation, with a weight loss of 0.96 % at 285 °C. As the crosslinker content increases, the degradation profile transitions into a three-stage process, indicating a higher degree of crosslinking and improved thermal stability. The main degradation of the E-PCSL resin occurs between 285 and 337 °C. Beyond 30 wt.% CA, the crosslink density significantly increases, forming a more robust network that hinders volatilization and depolymerization, thereby enhancing heat resistance. In Fig. 7b, the M-FA composite exhibits a maximum weight loss of only 0.4 %, with its primary thermal degradation occurring between 380–426 °C. The enhanced thermal stability, relative to the pristine E-PCSL resin, results from the effective physical barrier formed by the well-dispersed M-FA, which hinders the release of volatile degradation by products. Additionally, the thermal stability of the M-FA composite is shown to increase compared to the U-FA composite due to PDA modification. This suggests superior bonding with the E-PCSL30 resin due to improved interface adhesion resulting from FA modification. The presence of thermally stable silica and alumina phases in FA

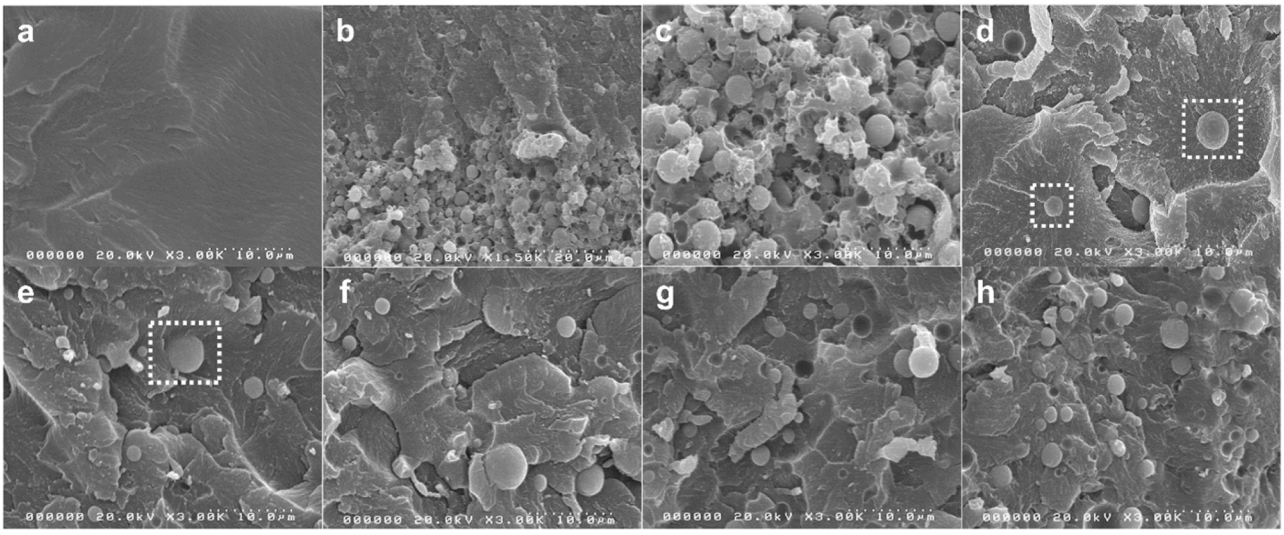

Fig. 6. SEM micrographs of Cross-sectional surfaces: (a) Pure E-PCSL30 resin, (b, c) U-FA composites (0.1 wt.%) showing sedimentation and smooth pull-out voids; (d–h) M-FA composites with varying contents: (d) 0.1 wt.%, (e) 0.25 wt.%, (f) 0.5 wt.%, (g) 1.25 wt.%, and (h) 2.5 wt.%.

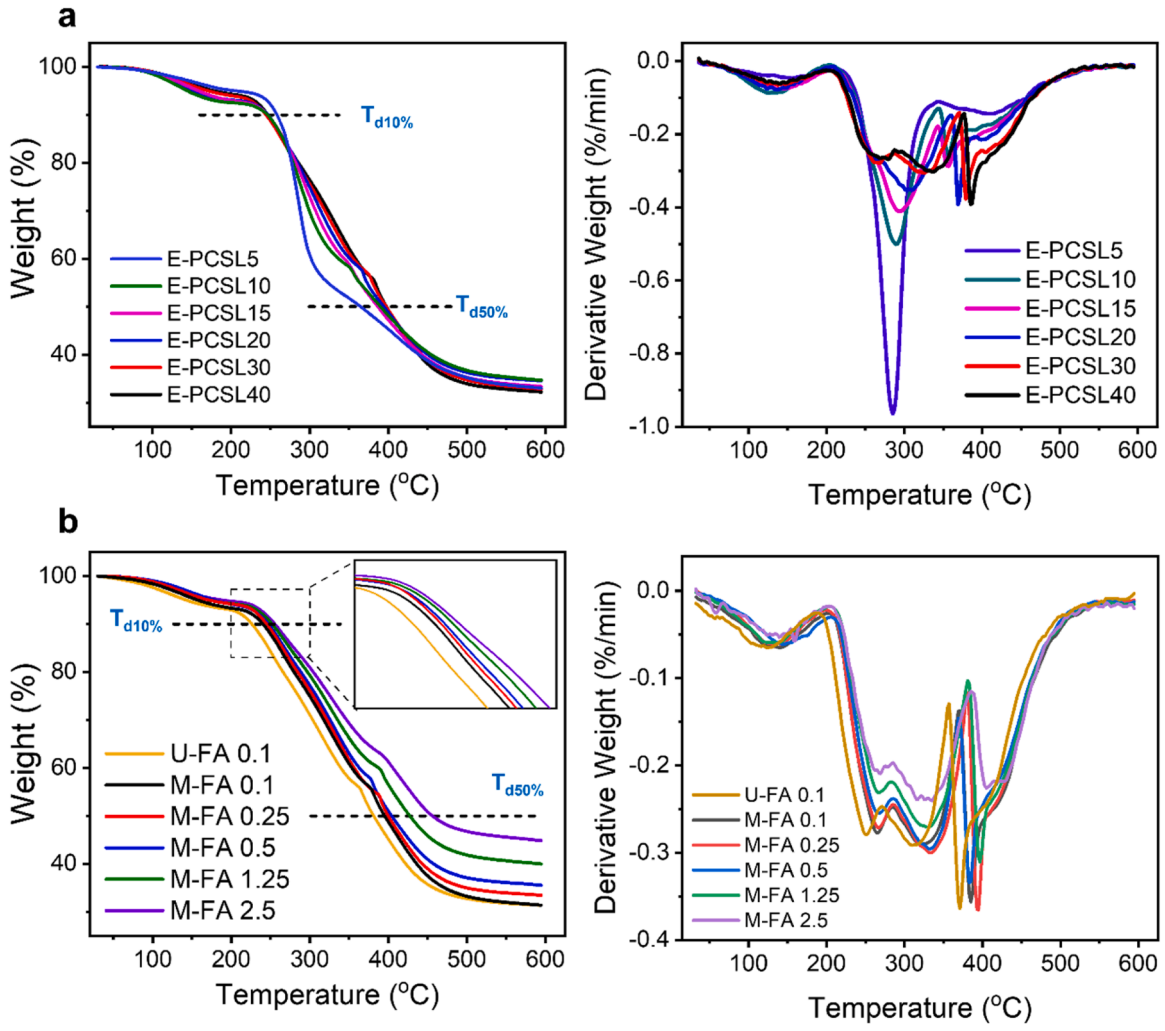

Fig. 7. TGA and DTG curves of (a) E-PCSL resin; (b) U-FA and M-FA/EPCSL30 composites.

also plays a key role in resisting early decomposition and improving the composite's overall heat resistance. Consistent with these mechanisms, previous studies have demonstrated that employing very high loadings of FA can further maximize the overall thermal stability of polymer

Table 4
TGA analysis of E-PCSL resin, U-FA, and M-FA/EPCSL30 composites.

Sample name		Decomposition ($T_{d10\ \%}$)	Decomposition ($T_{d50\ \%}$)
Resin	**E-PCSL5**	257.34	362.97
	E-PCSL10	247.41	386.87
	E-PCSL15	246.42	388.86
	E-PCSL20	245.45	392.84
	E-PCSL30	241.46	396.82
	E-PCSL40	239.48	398.82
Composite	**U-FA0.1**	225.57	380.89
	M-FA0.1	242.48	398.83
	M-FA0.25	245.42	400.82
	M-FA0.5	247.41	404.81
	M-FA1.25	253.36	428.75
	M-FA2.5	257.34	456.63

composites, as the abundant inorganic particles act as a more robust physical barrier against heat and mass transfer [33]. Table 4 summarizes thermal properties of the resins and composites.

3.7. Dynamic mechanical properties

Subsequently, the temperature-dependent storage modulus and loss factor (tan δ) profiles of the fabricated composites were evaluated, as depicted in Fig. 8. These specific thermo-mechanical metrics are essential for elucidating the inherent viscoelastic nature and dynamic structural responses of polymeric matrices [34]. In the low-temperature regime, all samples exhibit high storage modulus values, reflecting their inherent stiffness and solid-like character. Within this glassy state, the polymer chains remain frozen with limited segmental mobility. However, as the temperature approaches the glass transition zone, a sharp decline in stiffness occurs, triggered by the onset of cooperative segmental motion. Finally, in the rubbery plateau, the storage modulus stabilizes as the chain movement is constrained by the chemically crosslinked network.

To quantify the mechanical stiffness across different thermal states, the storage modulus values at 25 °C (glassy state) and 100 °C (rubbery plateau) were compared for all samples. First, the pure E-PCSL30 resin exhibited storage modulus values of 3.89 ± 0.03 GPa at 25 °C and 1.82 ± 0.05 GPa at 100 °C. Second, the incorporation of 0.1 wt.% U-FA (U-FA0.1) resulted in a decrease in stiffness, showing values of 3.33 ± 0.23 GPa at 25 °C and 1.76 ± 0.04 GPa at 100 °C. This reduction compared to the pure resin is attributed to the poor dispersion and adhesion of U-FA within the matrix. In contrast, the composite containing 0.1 wt.% M-FA (M-FA0.1) achieved the highest performance, reaching 4.07 ± 0.31 GPa at 25 °C and 1.89 ± 0.09 GPa at 100 °C. To further investigate the reinforcing effect and interfacial interactions at higher filler loadings, the 2.5 wt.% composites were also evaluated. The U-FA2.5 composite exhibited increased stiffness with storage modulus values of 4.80 ± 0.07 GPa at 25 °C and 2.57 ± 0.08 GPa at 100 °C. However, the M-FA2.5 composite demonstrated the highest mechanical performance, achieving 5.05 ± 0.04 GPa at 25 °C and 2.79 ± 0.04 GPa at 100 °C. The significant improvement in the storage modulus after FA modification, particularly at higher loadings, shows that the composites can effectively withstand the loading through good dispersion and strong bonding with the polymer matrix. Furthermore, previous studies investigating very high loadings of FA have similarly reported an increase in storage modulus up to an optimal filler concentration, after which the mechanical performance tends to decline [35].

Regarding the glass transition temperature (T_g), identified by the position of the tan δ peak maxima in Fig. 8b, the peaks shifted to higher temperatures in the composites. The specific T_g values were 82.24 °C for the pure resin, 84.75 °C for U-FA0.1, and 87.24 °C for M-FA0.1. In the case of the 2.5 wt.% composites, U-FA2.5 showed a T_g of 84.74 °C, which is similar to that of U-FA0.1. In contrast, M-FA2.5 exhibited a substantial increase, reaching a T_g of 89.79 °C. The reasons for this are the formation of hydrogen bonds as they interact with the surface of FA, and the structural changes that make chain movement restricted, resulting in a higher T_g [36]. Additionally, the intensity of the tan δ peak

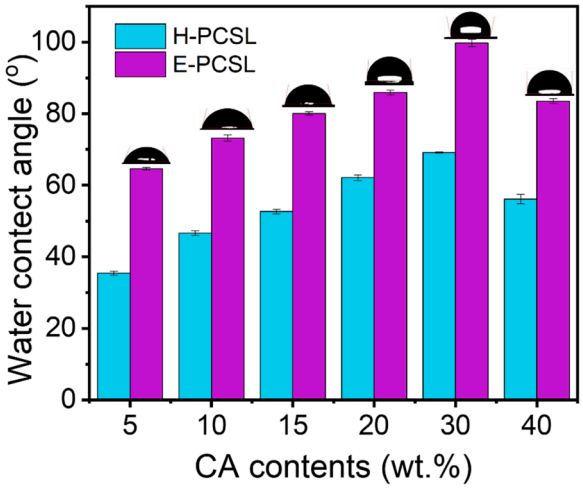

Fig. 9. Hydrophobic properties of H-PCSL and E-PCSL resins as measured by WCA.

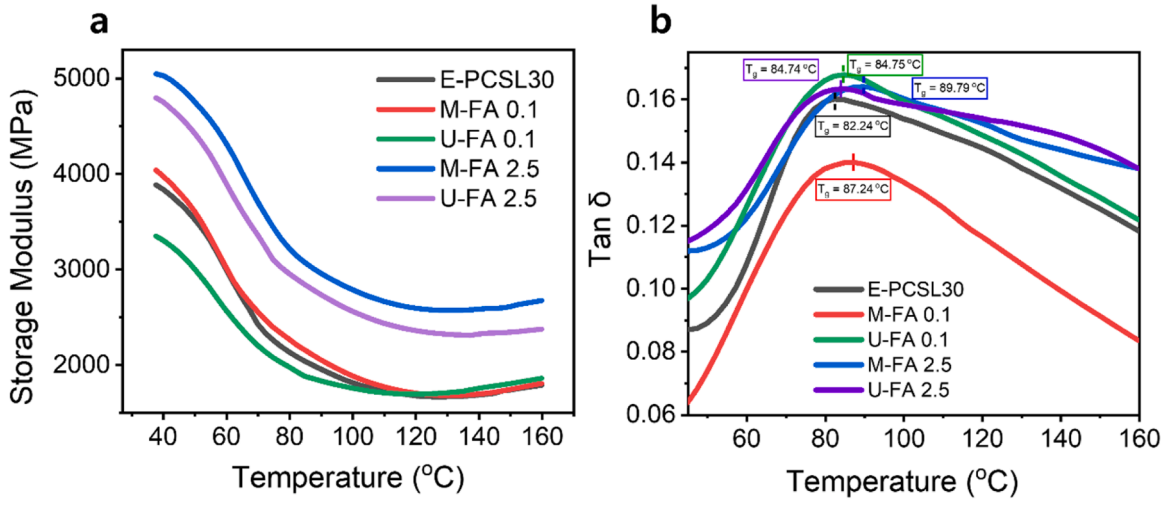

Fig. 8. Dynamic mechanical analysis of E-PCSL30 resin, U-FA0.1, 2.5 and M-FA0.1, 2.5 composites.

was notably suppressed for the M-FA composites, indicating that the strong interfacial interactions significantly constrain the polymer network and reduce energy dissipation.

3.8. Surface wettability of resins

Surface wettability is a critical factor influencing resin performance and was therefore evaluated through WCA measurements, as shown in Fig. 9. The H-PCSL resin exhibited a WCA ranging from 32.82 to 69.18 (±0.9°), which was significantly lower than that of the esterified E-PCSL resin (64.59 to 99.81±1.1°). This increase in WCA is attributed to a reduction in hydroxyl (-OH) groups in E-PCSL due to esterification. Notably, E-PCSL30 showed a 44.3 % improvement in WCA compared to H-PCSL30, indicating a significant transition towards enhanced hydrophobicity. This improvement results from two synergistic mechanisms.

First, chemically, the esterification replaces highly polar hydroxyl (-OH) and carboxyl groups with less polar ester groups, lowering the surface energy. Second, physically, the increased crosslinking density creates a denser polymer network which undergoes curing shrinkage, inducing micro-scale surface roughness on the matrix. According to the Wenzel model, this roughness amplifies the hydrophobicity of the resin [37].

In the composite system, this roughness is further intensified by the M-FA fillers. The mismatch between the shrinking matrix and the rigid particles creates localized protrusions and a hierarchical texture. Consequently, the chemically and physically engineered resin matrix serves as the fundamental barrier against water permeation.

4. Conclusions

In this study, high-performance Eco-friendly composites, characterized by superior tensile strength (>140 MPa) and thermal stability comparable to that of engineering plastics, were successfully developed by combining a novel E-PCSL30 resin with M-FA.

The Optimization of Eco-friendly Resin was achieved by formulating a composition containing 30 wt.% citric acid as a green crosslinker, followed by curing at 180 °C for 18 h. This process established a dense thermoset network via esterification of PVA and sodium lignosulfonate, yielding a structurally stable matrix. In contrast to U-FA, M-FA demonstrated homogeneous dispersion and robust interfacial adhesion. This enhancement is attributed to the synergistic interplay of catechol-metal coordination and hydrogen bonding, which facilitates efficient stress transfer within the composite system.

The incorporation of 0.1 wt.% M-FA yielded the most balanced property profile. The composites maintained a high tensile strength of 144.8 MPa while exhibiting superior elongation at break (9.5 %), Young's modulus (4.3 GPa), and toughness (9.81 MJ/m^3). Additionally, the ester-crosslinked network and M-FA incorporation significantly enhanced the high-temperature stability. The development of a stable char layer acts as a thermal barrier, effectively shielding the matrix and retarding degradation, though this benefit involves a trade-off in initial decomposition temperature due to moisture dehydration.

As a sustainable alternative to conventional petrochemical engineering plastics, the developed composite demonstrates considerable potential for semi-structural automotive exterior and interior parts, functional thermal barrier coatings, high-stiffness sustainable packaging materials, eco-friendly construction materials, and electronic enclosures. This approach provides a viable pathway for upcycling industrial waste into high-value performance materials. Regarding the circularity and end-of-life management of the thermoset matrix, the ester-based crosslinking structure inherent in the E-PCSL30 resin offers potential for chemical recycling via hydrolysis or biodegradation under specific conditions, unlike traditional irreversible thermosets. This feature, combined with the valorization of industrial waste (FA), supports a closed-loop approach to sustainability.

While this study successfully demonstrated the synthesis and high performance of E-PCSL30/M-FA composites via a laboratory-scale petri dish casting method, this water-based process is fundamentally highly compatible with industrial continuous manufacturing techniques. Specifically, the aqueous resin system can be readily scaled up using continuous slot-die coating, aqueous tape casting, or roll-to-roll (R2R) processing for mass production. Future research will aim to bridge the gap toward industrial application. Key focus areas will include optimizing pilot-scale processing for mass production and evaluating long term durability and specific biodegradability/recyclability under various environmental conditions to further validate the material's commercial versatility and sustainability credentials.

CRediT authorship contribution statement

Giseok Park: Writing – original draft, Methodology, Investigation, Data curation, Conceptualization. **Sunanda Roy:** Visualization, Resources, Methodology. **Jung Woong Kim:** Validation, Investigation, Data curation. **Hyun Chan Kim:** Software, Funding acquisition, Formal analysis, Conceptualization. **Jaehwan Kim:** Writing – review & editing, Supervision, Methodology, Conceptualization.

Declaration of competing interest

The authors declare that they have no known competing financial interests or personal relationships that could have appeared to influence the work reported in this paper.

Acknowledgments

This work was supported by the National Research Foundation of Korea (NRF) grant funded by the government (Ministry of Science and ICT) (RS-2024-00353023).

Data availability

Data will be made available on request.

References

[1] D.K. Nayak, P.P. Abhilash, R. Singh, R. Kumar, V. Kumar, Fly ash for sustainable construction: a review of fly ash concrete and its beneficial use case studies, Clean. Mater. 6 (2022) 100143, https://doi.org/10.1016/j.clema.2022.100143.
[2] E.R. Teixeira, A. Camões, F.G. Branco, Synergetic effect of biomass fly ash on improvement of high-volume coal fly ash concrete properties, Constr. Build. Mater. 314 (2022) 125680, https://doi.org/10.1016/j.conbuildmat.2021.125680.
[3] H. Yangthong, K. Buaksuntear, S. Suethao, A. Chworos, W. Smitthipong, Waste material fly ash as an alternative filler for elastomers, Polym. Eng. Sci. 63 (2023) 2624–2644, https://doi.org/10.1002/pen.26400.
[4] H. Yangthong, P. Udomsin, S. Jansinak, S. Suethao, K.L. Goh, W. Smitthipong, Sustainable use of fly ash waste in tire tread rubber: characterization of physical properties and environmental impact assessment, Waste Manag. 200 (2025) 114737, https://doi.org/10.1016/j.wasman.2025.114737.
[5] A. Pattanaik, M. Mukharjee, S.C. Mishra, Effect of environmental aging conditions on the properties of fly ash filled epoxy composites, Adv. Compos. Mater. 29 (2020) 1–30, https://doi.org/10.1080/09243046.2019.1610930.
[6] A.M.A. Mohammed Altaweel, C. Ranganathaiah, B. Kothandaraman, J.M. Raj, M. N. Chandrashekara, Characterization of ACS modified epoxy resin composites with fly ash and cenospheres as fillers: mechanical and microstructural properties, Polym. Compos. 32 (2011) 139–146, https://doi.org/10.1002/pc.21030.
[7] M. Gnanavel, T. Maridurai, K. KM, Mechanical, thermal and dielectric behaviour of C-class fly-ash coarse and fine particles reinforced epoxy resin composite, Mater. Res. Express. 6 (2019) 095507, https://doi.org/10.1088/2053-1591/ab2e50.
[8] T. Wongwuttanasatian, W. Chaochaiyaphum, V. Seithtanabutara, Valorization of MSW incinerator fly ash for epoxy-based composite for interior light partition application, Waste Biomass Valor 13 (2022) 2795–2814, https://doi.org/10.1007/s12649-022-01684-2.
[9] A. Pattanaik, M. Mukherjee, S.B. Mishra, Influence of curing condition on thermo-mechanical properties of fly ash reinforced epoxy composite, Compos. Part B Eng. 176 (2019) 107301, https://doi.org/10.1016/j.compositesb.2019.107301.
[10] L. Su, Y. Zhang, Q. Du, X. Dai, J. Gao, P. Dong, et al., An experimental study on the removal of submicron fly ash and black carbon in a gravitational wet scrubber with electrostatic enhancement, RSC Adv. 10 (2020) 5905–5912, https://doi.org/10.1039/C9RA10046F.

[11] S. Roy, L.V. Hai, J. Kim, Synergistic effect of polydopamine–polyethylenimine copolymer coating on graphene oxide for EVA nanocomposites and high-performance triboelectric nanogenerators, Nanoscale Adv. 1 (2019) 2444–2453, https://doi.org/10.1039/C9NA00142E.
[12] S.S. Ruppel, J. Liang, Tunable properties of polydopamine nanoparticles and coated surfaces, Langmuir 38 (2022) 5020–5029, https://doi.org/10.1021/acs.langmuir.2c00719.
[13] G. Kafkopoulos, E. Karakurt, R.P. Martinho, J. Duvigneau, G.J. Vancso, Engineering of adhesion at metal–poly(lactic acid) interfaces by poly(dopamine): the effect of the annealing temperature, ACS Appl. Polym. Mater. 5 (2023) 5370–5380, https://doi.org/10.1021/acsapm.3c00672.
[14] Z. Ahmad, Y. Yusof, H. Anuar, R. Khairul, The effect of water and citric acid on sago starch bio-plastics, Int. Food Res. J. 19 (2012) 715–719.
[15] T. Aro, P. Fatehi, Production and application of lignosulfonates and sulfonated lignin, ChemSusChem 10 (2017) 1861–1877, https://doi.org/10.1002/cssc.201700082.
[16] S. Roy, H.D. Pham, M. Latif, J.W. Kim, G. Park, J. Kim, et al., Facile and sustainable upcycling of fly ash into multifunctional durable superhydrophobic coatings, Prog. Org. Coat. 197 (2024) 108770, https://doi.org/10.1016/j.porgcoat.2024.108770.
[17] T. Stern, P. Schwarzbauer, Wood-based lignosulfonate versus synthetic polycarboxylate in concrete admixture systems: the perspective of a traditional pulping by-product competing with an oil-based substitute in a business-to-business market in central Europe, For. Prod. J. 58 (2008) 81–86.
[18] H.U. Ko, J.W. Kim, H.C. Kim, L. Zhai, J. Kim, Esterified PVA-lignin resin by maleic acid applicable for natural fiber reinforced composites, J. Appl. Polym. Sci. 137 (2020) 48836, https://doi.org/10.1002/app.48836.
[19] Y. Zhang, F. Meng, Z. Hu, Y. Jia, Z. Chen, H. Fei, et al., A novel bio-mass resveratrol-modified lignin-based phenolic resin with high glass transition temperature and improved mechanical properties, J. Polym. Environ. 32 (2024) 4986–5000, https://doi.org/10.1007/s10924-024-03290-w.
[20] Q. Ma, G. Zheng, J. Jiang, W. Fan, S. Ge, Recycling of waste bamboo biomass and papermaking waste liquid to synthesize sodium lignosulfonate/chitosan glue-free biocomposite, Molecules 28 (2023) 6058, https://doi.org/10.3390/molecules28166058.
[21] H.U. Ko, L. Zhai, J.H. Park, J.Y. Lee, D. Kim, J. Kim, Poly(vinyl alcohol)–lignin blended resin for cellulose-based composites, J. Appl. Polym. Sci. 135 (2018) 46655, https://doi.org/10.1002/app.46655.
[22] J. Sun, C. Wang, J.C.C. Yeo, D. Yuan, H. Li, L.P. Stubbs, et al., Lignin epoxy composites: preparation, morphology, and mechanical properties, Macromol. Mater. Eng. 301 (2016) 328–336, https://doi.org/10.1002/mame.201500310.
[23] D.O. Agumba, P.S. Panicker, D.H. Pham, J. Kim, Advanced green thermoset resin tailored for nanocellulose-based filament-reinforced polymer composite and sustainable development, Adv. Sustain. Syst. 6 (2022) 2200369, https://doi.org/10.1002/adsu.202200369.
[24] M.N. Alghamdi, Performance for fly ash reinforced HDPE composites over the ageing of material components, Polymers 14 (2022) 2913, https://doi.org/10.3390/polym14142913. . (Basel).
[25] A.W. Nugroho, M.K.P. Prasetyo, C. Budiyantoro, Effect of fly ash on the mechanical properties of polyvinyl chloride-fly ash composite, in: U. Sabino, F. Imaduddin, A. R. Prabowo (Eds.), Proceedings of the 6th International Conference and Exhibition on Sustainable Energy and Advanced Materials, Singapore, Springer, 2020, pp. 667–674, https://doi.org/10.1007/978-981-15-4481-1_63.
[26] W. Yao, Y. Zhao, K. Wu, L. Han, H. Cai, W. Guo, Effect of fly ash on the structure and properties of polyolefin elastomer/fly ash/polypropylene composites, Mater. Res. Express. 6 (2018) 025308, https://doi.org/10.1088/2053-1591/aaed18.
[27] A.K. Maurya, R. Gogoi, S.K. Sethi, G. Manik, A combined theoretical and experimental investigation of the valorization of mechanical and thermal properties of the fly ash-reinforced polypropylene hybrid composites, J. Mater. Sci. 56 (2021) 16976–16998, https://doi.org/10.1007/s10853-021-06383-2.
[28] C. Wu, Y. Yang, B. Pang, Y. Cui, The effect of different particle sizes of fly ash on the properties of mortar, Materials 18 (2025) 4693, https://doi.org/10.3390/ma18204693. . (Basel).
[29] T.F. Silva da, F. Menezes, L.S. Montagna, A.P. Lemes, F.R. Passador, Effect of lignin as accelerator of the biodegradation process of poly(lactic acid)/lignin composites, Mater. Sci. Eng. B 251 (2019) 114441, https://doi.org/10.1016/j.mseb.2019.114441.
[30] M. Wądrzyk, R. Janus, M. Lewandowski, A. Magdziarz, On mechanism of lignin decomposition – investigation using microscale techniques: Py-GC–MS, Py-FT-IR and TGA, Renew. Energy 177 (2021) 942–952, https://doi.org/10.1016/j.renene.2021.06.006.
[31] C. Liu, B. Yuan, M. Guo, Q. Yang, T.T. Nguyen, X. Ji, Effect of sodium lignosulfonate on bonding strength and chemical structure of a lignosulfonate/chitosan-glutaraldehyde medium-density fiberboard adhesive, Adv. Compos. Hybrid. Mater. 4 (2021) 1176–1184, https://doi.org/10.1007/s42114-021-00351-9.
[32] M. Inada, H. Tsujimoto, Y. Eguchi, N. Enomoto, J. Hojo, Microwave-assisted zeolite synthesis from coal fly ash in hydrothermal process, Fuel 84 (2005) 1482–1486, https://doi.org/10.1016/j.fuel.2005.02.002.
[33] S. Sengupta, D. Ray, A. Mukhopadhyay, Sustainable materials: value-added composites from recycled polypropylene and fly ash using a green coupling agent, ACS Sustain. Chem. Eng. 1 (2013) 574–584, https://doi.org/10.1021/sc3000948.
[34] W.K. Goertzen, M.R. Kessler, Dynamic mechanical analysis of carbon/epoxy composites for structural pipeline repair, Compos. Part B Eng. 38 (2007) 1–9, https://doi.org/10.1016/j.compositesb.2006.06.002.
[35] S. Sengupta, K. Pal, D. Ray, A. Mukhopadhyay, Furfuryl palmitate coated fly ash used as filler in recycled polypropylene matrix composites, Compos. Part B Eng. 42 (2011) 1834–1839, https://doi.org/10.1016/j.compositesb.2011.06.021.
[36] A.S. Mora, R. Tayouo, B. Boutevin, G. David, S. Caillol, Vanillin-derived amines for bio-based thermosets, Green Chem. 20 (2018) 4075–4084, https://doi.org/10.1039/C8GC02006J.
[37] M.S. Bell, A. Borhan, A volume-corrected Wenzel model, ACS Omega 5 (2020) 8875–8884, https://doi.org/10.1021/acsomega.0c00495.